Hindawi
International Journal of Chemical Engineering
Volume 2021, Article ID 7762127, 16 pages
https://doi.org/10.1155/2021/7762127

Research Article

Investigations of Structural and Residual Trapping Phenomena during CO_2 Sequestration in Deccan Volcanic Province of the Saurashtra Region, Gujarat

Pradeep Reddy Punnam, Balaji Krishnamurthy, and Vikranth Kumar Surasani

Department of Chemical Engineering, Birla Institute of Technology and Science, Pilani Hyderabad Campus, Hyderabad 500078, India

Correspondence should be addressed to Vikranth Kumar Surasani; surasani@hyderabad.bits-pilani.ac.in

Received 15 April 2021; Accepted 18 June 2021; Published 8 July 2021

Academic Editor: Ho SoonMin

This work aims to study the structural and residual trapping mechanisms on the Deccan traps topography to elucidate the possible implementation of CO_2 geological sequestration. This study provides an insight into a selection of stairsteps landscape from Deccan traps in the Saurashtra region, Gujarat, India. Various parameters affect the efficiency of the structural and residual trapping mechanisms. Thus, the parametric study is conducted on the modeled synthetic geological domain by considering the suitable injection points for varying injection rates and petrophysical properties. The outcomes of this study will provide insights into the dependencies of structural and residual trapping on the Deccan traps surface topography and injection rates. It can also establish a protocol for selecting the optimal injection points with the desired injection rate for the safe and efficient implementation of CO_2 sequestration. The simulation results of this study have shown the dependencies of structural and residual trapping on the geological domain parameters.

1. Introduction

According to the International Energy Agency (IEA), the atmospheric CO_2 concentration has reached an alarming level of 410 ppm, in which the energy-related CO_2 emissions rose to a historic high [1]. The increase in the CO_2 concentration has led to a rise in the average temperature on the Earth's surface, resulting in deleterious phenomena like the melting of ice caps in polar regions, thereby creating ecological imbalance. Scientists and researchers are looking for various measures to reduce the effects of CO_2 and control global warming to an extent by reducing the amount of CO_2 reaching the atmosphere [2]. Among the significant measures, CO_2 sequestration is a promising strategy to reduce carbon emissions. CO_2 sequestration is the only storage technique that reduces the CO_2 concentration in the atmosphere without reducing the consumption of fossil fuels, and it is becoming popular among researchers and environmentalists [3]. CO_2 storage requires careful consideration of location and effective predictive analysis [4]. Depending on the storage types, CO_2 sequestration is classified into geologic sequestration, ocean sequestration, and terrestrial sequestration. Geologic sequestration involves storing captured CO_2 in deep geologic formations. Some suitable geologic formations for storage are mature oil and gas reservoirs, coal beds, saline aquifers, and basalt formations [3–5]. This work aims to simulate CO_2 geological sequestration in Deccan volcanic province.

The Deccan volcanic province in India is spread across 5,00,000 km^2 [6]. Its petrophysical and geochemical properties are considered one of the largest sinks for the CO_2 geological sequestration [7]. In 1970, the Indian government planned to store nuclear waste in these traps, but the idea was abandoned due to water contamination possibilities [8]. An old survey conducted by the Indian government in collaboration with Pacific Northwest National Laboratory

(PNNL) estimated that about 150 gigatons of CO_2 could be stored in the Deccan volcanic provinces with strategic implementation of CO_2 sequestration [8]. The Deccan volcanic basalt rock layers are formed due to the cooling and solidification of molten lava, which came out due to volcanic eruption at the end of the Cretaceous period [9, 10]. There are nearly 11 types of basalt rock formations found in India. These basalt rock formations are somewhat similar to the basalt formation found in Iceland and Columbia River basalts of the north-western United States [11–13]. The geological subsurface arrangement of the Basalt layers and Mesozoic sediment layers with other geological layers made Deccan volcanic provinces the exemplary candidate for the CO_2 geological sequestration [7]. Deccan volcanic province possesses vast geological heterogeneity with a sequential arrangement of basalt layers with the availability of vesicular basalt and massive basalt. The massive basalt layer should act as caprock due to its fault-free and thick enough layer so that it can act as an impermeable seal [7]. The mineral composition of the Deccan basalts is dominated by the Pyroxene, Plagioclase, and Olivine mineral groups [11, 14–17]. Basalt rock formation consists mainly of the divalent cation like Ca^{2+}, Mg^{2+}, and Fe^{2+}, which is advantageous in forming the secondary minerals. When these divalent cations react with dissolved CO_2, minerals like calcite, magnesite, and siderite are formed [11, 12, 15, 17, 18]. Due to the availability of favorable minerals, Deccan traps can be considered a potential candidate for CO_2 sequestration. The Deccan volcanic region considered in this work is based on the Saurashtra Peninsula with the precise location of 21.50° N–23° N and 69.75° E–71.50° E longitude [19]. The major part of the Saurashtra Peninsula is excepted to be covered by the Deccan traps.

The fate of injected CO_2 during the geological sequestration is classified into four categories. First, when the CO_2 is injected into the domain, the formation's top impermeable layer provides the primary trap. It prevents CO_2 from escaping to Earth's surface; this type of trapping mechanism is called structural trapping. The second is residual trapping, where CO_2 migrating through a porous medium gets trapped in the migration pathway or confined inside a porous structure. The third is solubility trapping; the residual CO_2 will interact with resident water to solubilize and form weak carbonic acid. The fourth is mineral trapping; the weak carbonic acid will begin to react with mineral rocks and form secondary carbonate minerals [20].

The efficiency of the CO_2 geological sequestration is determined by structural and residual trapping mechanisms [21]. Therefore, understanding the movement of CO_2 and its spreading in various forms is vital for a specific geological formation. As more CO_2 gets trapped in the rigid porous formation, a higher amount of CO_2 will undergo solubility trapping leading to a surge in the production of carbonic acid, which leads to an increase in the mineral reaction and mineral trapping in the formation domain [22, 23]. The obtained percentages of structural and residual trapping results can provide a vigorous interpretation for the solubility and mineral trapping. Therefore, this article aims to enhance the understanding of the structural and residual trapping mechanisms for CO_2 sequestration in the Deccan volcanic formation domain. Investigation on structural and residual trapping alone will help understand the fate of CO_2 in the geological formation and assist in further studies on the field-scale application [24].

In situ pressures and temperatures of deep geological formations are favorable to operate the geological sequestration process in the supercritical state. The main advantage of storing CO_2 in a supercritical state ($ScCO_2$) is that it consumes less storage volume than the CO_2 present in the gaseous state. Furthermore, in this article, the reference CO_2 means the carbon dioxide is present in a supercritical state. The CO_2 injected at the deepest geological formation will remain in the supercritical condition due to in situ pressures and temperatures [23, 25, 26]. When injected into the deep subsurface formation, CO_2 in the form of a plume tends to move upwards due to the buoyancy force. In this process, while injecting CO_2 percolate through the formation layer, it encounters porous channels and traps and leaves residuals in the migration pathway [27, 28]. The traps are within the more prominent geological formation, which serves as storage spaces or minireservoirs [29].

To explain the structural and residual trapping phenomena, a geological formation is considered, as illustrated in Figure 1(a). Most of the naturally formed formation layers contain geological perturbations. In geological terminology, it is typically referred to as anticline and syncline sequences. When the injected CO_2 tends to move laterally with the top surface, these perturbations of anticline and syncline primarily affect the migration and movement of the CO_2 plume. These perturbations of the geological domain act as a trap, which restricts the movement of CO_2 in the anticline dome. This phenomenon further contributes to the trapping mechanisms of CO_2 sequestration [30–32]. The injected CO_2 forms a plume that will move upwards due to buoyancy; this phenomenon is pictorially represented in Figure 1(a). The CO_2 plume displaces water and moves freely in the formation domain with the influences of injection pressure; this quantity of CO_2 plume is classified as *movable plume*; see Figure 1(b). The CO_2 plume moves upwards and gets restricted by an impermeable layer, caprock, and starts moving in the lateral direction. The part of the plume that comes under the influence of caprock will lose its momentum and spread in the lateral direction; see Figure 1(c). During injection, CO_2 accumulated under the one anticline dome will overflow to the next anticline dome. which causes CO_2 movement under the caprock; see Figures 1(d) and 1(e). After the injection period, the CO_2 under the caprock will lose its momentum and get structurally trapped under the anticline domes. This quantity of CO_2 is classified as *structural trapping*. In the postinjection period (Figure 1(e)), movable plume starts losing momentum and tends to be trapped in the geological domain. The appreciable amount of CO_2 gets trapped in the migration pathway during the upward movement of the plume and is confined inside the porous structure. This quantity of trapped CO_2 is classified as *residual trapping*. The fate of CO_2 injection during the postinjection period over the geological time is shown in Figure 1(e). After the injection of CO_2, there is an apparent

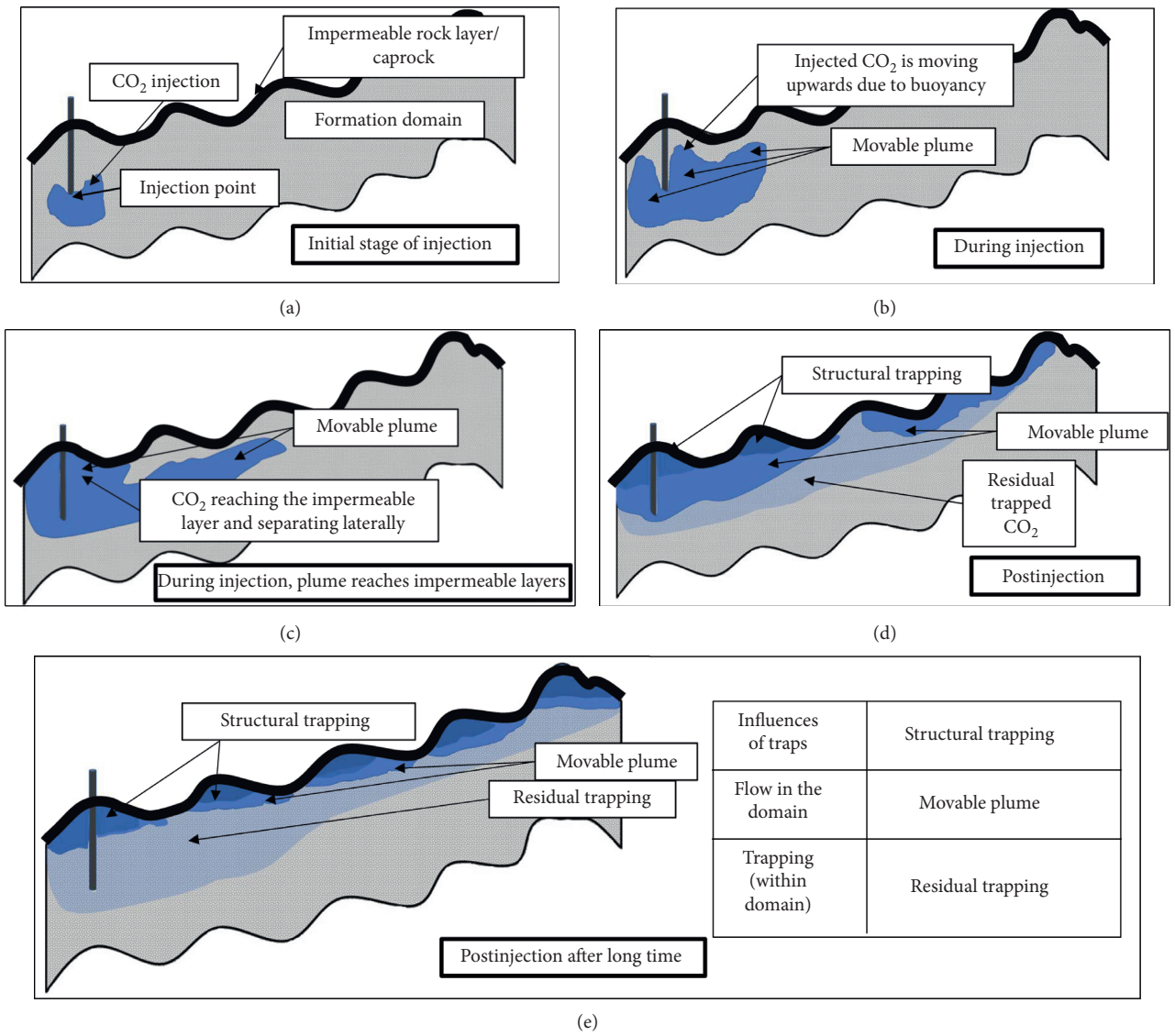

Figure 1: Classification of the structural trapping and residual trapping mechanisms during geological sequestration: (a–e) the fate of CO_2 during injection and after injection in the geological formation.

transformation of the movable plume to structural and residual trapping. The residual trapped CO_2 coexist with water, solubilized in water to interact with minerals in the formations. Therefore, an increase in the percentage of residuals in the formation domain is favorable to CO_2 solubility and then to mineralization [31, 33, 34].

Most of the research conducted on the structural and residual trapping mechanisms is taken with the aspect of CO_2 saturation to estimate the trapping efficiency in the geological domain [31, 33, 35, 36]. The parameters considered in their studies mostly deal with the reservoir parameters such as pore aspect ratio [37, 38], rock type [39], capillary pressure [40–42], saturation [27, 43], porosity [33], and flow rate [44, 45]. In the pore aspect ratio study, the influences of the pore size and throat size of the porous domain are studied on the trapping mechanism and plume migration [37, 38]. The influences of the rock structure and rock composition on CO_2 entrapment (both structural and residual trapping) are studied [39]. The influences of porosity are studied regarding the saturation distribution of nonwetting fluid and variation on capillary pressure of the domain [33, 40–42, 46, 47]. Most of these studies were conducted with numerical simulations or/and experimental investigation under controlled parameters by considering the core samples of the geological domain [31, 48]. Most researchers use experimental techniques like core-flooding techniques and X-ray microtomography to study the trapping capacity at the lab scale [27, 44, 46, 49].

In the literature, research is conducted on geomorphological structures to study their influences and impact on the structural and residual trapping mechanisms. The SINTEF researchers have developed a reservoir toolbox called MRST-co2lab [33], which can study the influences of the various topographical formations of the Norwegian continental shelf. The techniques like vertical equilibrium and spill-point analysis were used to evaluate and estimate trapping and storage

capacities of various formations [31, 50]. Nearly the topographies of 14 geological formations are saved in this toolbox, in which some of the popular formation topographies are Sleipner [33, 51], Sandes [33, 52], Utsira [22, 32], and Statfjord [33, 50]. Nilsen et al. [53] conducted a study on the combined stratigraphic scenarios of different formation morphologies by considering the flooded marginal marine setting and buried offshore sand ridges structures. The spill-point analysis was carried out to analyze the influences of the migration pathway. Moreover, this study is carried out by examining the structural and residual trapping percentages. The author in this research concluded that the uncertainty on top-surface morphology has a clear impact on the CO_2 migration and structural and residual trapping entrapment [53]. Allen et al. [52] performed a similar simulation analysis on the Utsira and Sandnes formations. The study was focused on the caprock elevation, migration of CO_2, and petrophysical properties. Additionally, the perturbation influences on the topography of the formations were explained with a synthetic smooth and wavy top surface of a domain. It was found that the topographical perturbations and caprock elevation have an impact on the structural trapping percentage and CO_2 migration in the domain [52]. Ahmadinia et al. [54] conducted a simulation study on a top-surface structure shaped as a sinusoidal wave. This research by the author was conducted to study the influences of the sloping nature of an aquifer. The structural, residual, and solubility trapping percentages were considered a parameter of evaluation to study the influences of the sloping angle of the top surface. It was observed that the dissolution of CO_2 was less in the highly tilted formation domain due to the uncertainty in residual trapping in the lower formation layers [54].

In this current research, for the first time, a stairsteps kind of structure is considered to conduct a simulation analysis to study the influences of the topography of Deccan traps located in the Saurashtra region, India [19]. This numerical study will provide insight into selecting the injection point and injection rate at the safe range of petrophysical properties to safely implement CO_2 sequestration in the Deccan volcanic province. To achieve this, first, the synthetic geological domain of Deccan traps is modeled. Then, the appropriate boundary conditions and petrophysical properties are assigned to the simulation domain. Further, the CO_2 sequestration simulations are carried out at various injection rates, injection points, and petrophysical properties. The structural and residual trapping percentages at discrete times are evaluated and studied. By illustrating the lateral movement of the injected CO_2 in the sizeable geological domain, it has provided an intuition on the influences of Deccan traps topography and geological parameters on the entrapment percentage of structural and residual trapping mechanism in geological time scale.

2. Model Description

Geological sequestration of CO_2 occurs in a subsurface porous structure that involves several processes, including flow and transport of CO_2. The solubility and mineral trapping mechanisms are neglected in this work to elucidate the influence of the structural and residual trapping mechanisms, meaning the transport due to chemical reactions is not considered.

2.1. Multiphase Flow Equations. Immiscible displacements of CO_2 and water are occurring in a complex porous geological formation at reservoir conditions. Each phase can involve more than one chemical species and can still be considered a single component because there is no mass transfer (dissolution of CO_2 in water) between phases. Hence, their compositions remain constant over a geological time scale. So, the incompressible flow is cogitated in the simulation domain [34]. The general mass conservation equations governing the multiphase flow is given by

$$\frac{\partial}{\partial t}\left(\varnothing \rho_\alpha S_\alpha\right) + \nabla.\left(\rho_\alpha \overrightarrow{\nu}_\alpha\right) = \rho_\alpha q_\alpha. \tag{1}$$

The subscript α denotes phases $\{l, g\}$ (where g is for CO_2 and l is for water). $\varnothing$ is the porosity; S_α and ρ_α are α phase saturation and density, respectively. The term $\overrightarrow{\nu}_\alpha$ is Darcy's velocity of α phase, which is given by

$$\overrightarrow{\nu}_\alpha = -K\frac{k_\alpha}{\mu_\alpha}\left(\nabla p - g\rho_\alpha \nabla z\right), \tag{2}$$

where K represents permeability, k_α represents relative permeability, μ_α is viscosity, and z is height. The following equation illustrates the saturation relation for all phases for a singular component:

$$\sum S_\alpha = 1. \tag{3}$$

2.2. Brooks–Corey Relation. The Brooks–Corey relation is used to relate the capillary pressure P_c to effective invading fluid saturation $S_{e\alpha}$. In this current simulation study, CO_2 is the invading fluid in the reservoir [34]. The Brooks–Corey relation is given by

$$S_{e,g} = \begin{cases} \left(\dfrac{P_c}{P_e}\right)^{-n_b}, & \text{if } P_c > P_e, \\ 1, & \text{if } P_c \le P_e, \end{cases} \tag{4}$$

where P_e is the entry pressure; P_c $(= (\rho_l - \rho_g)gh = \Delta\rho gh)$ is the capillary pressure; ρ_l and ρ_g are the densities of water and injected CO_2; $S_{e,g}$ is the effective CO_2 saturation; n_b is the parameter related to the pore size distribution. Its value is taken as 2.5, and its range is between 0.2 and 5 [34]. Brooks–Corey–Mualem model gives the relationship equation between relative permeability and effective saturation, as shown in the following equations.

$$\begin{aligned} k_{r,l} &= \left(S_{e,l}\right)^{n_1+n_2n_3}, \\ k_{r,g} &= \left(1 - S_{e,l}\right)^{n_1}\left[1 - \left(S_l\right)^{n_2}\right]^{n_3}, \end{aligned} \tag{5}$$

where n_1, n_2, and n_3 are constants, the value of n_1 is 1, n_2 is $1 + 1/n_b$, and n_3 is 2, which are obtained by the experimental fitting. From the above equation, $S_{e,l}$ is effective water saturation. The effective saturation fluid should be considered

normal saturation of fluid in this simulation analysis because it is considered that there is no presence of isolation pore space [34].

Further, the methodology for solving the equations is through discretization. Backward discretization along with discrete derivative operators for grad and div is defined to obtain the following implicit system of equations for a phase "α":

$$\frac{(\varnothing\rho_\alpha S_\alpha)^{n+1} - (\varnothing\rho_\alpha S_\alpha)^n}{\Delta t^n} + \operatorname{div}(\rho v)_\alpha^{n+1} = (\rho q)_\alpha^{n+1},$$
$$v_\alpha^{n+1} = \frac{-Kk_{r\alpha}}{\mu_\alpha^{n+1}}\left[\operatorname{grad}\left(p_\alpha^{n+1}\right) - g\rho_\alpha^{n+1}\operatorname{grad}(z)\right]. \tag{6}$$

The fluid movement is primarily defined by the action of buoyancy and capillary forces, which will govern the movement of injected CO_2 in the geological structure domain [34].

3. Numerical Modeling of the Synthetic Simulation Domain

3.1. Modeling the Synthetic Computation Domain. The domain considered in this research is the Saurashtra Peninsula with the precise location of 21.50°N–23°N and 69.75°E–71.50°E longitude adapted from Murthy et al. [19]. The major part of the Saurashtra Peninsula is excepted to be covered by the Deccan traps. The word "traps" in this context represent the stairsteps and stairsteps are like structures formed due to geological stretching, rifting, and uplifting happening from geological past [55] that happened nearly 65 million years ago [11, 56–58]. Figures 2(a)–2(c) illustrate the contour plot of the domain (see Figure 2(a) with high range stairsteps traps [19]. From Figures 2(b) and 2(c), a heavy dip can be seen at one corner of the domain. The dip section is related to the Kachchh rift, which shares its boundaries with the Saurashtra Peninsula. One can visualize and analyze the modeled domain as an integrated geomorphological structure of anticline dome and trap structure [11, 56–59].

The top surface of the domain is modeled by using the MATLAB image processing technique. First, by using the contour plot obtained by literature, the elevation of the structure is extracted. Then, by plotting the mesh grid in MATLAB, the top surface of the domain is modeled. Further, the whole grid structure is modeled and simulated using MRST-co2lab. The geological cracks and faults of the domain were not induced in the modeled domain to minimize the complexity of the simulation. The illustration of the synthetic simulation domain can be seen in Figure 2(d). The physical dimensions of the domain are 160 km × 160 km × 1.8 km. The domain is discretized into 2,56,000 (160 × 160 × 10) grid cells. An attempt was made to model the domain to an accurate demonstration of the realistic case.

3.2. Petrophysical Properties. The petrophysical properties, i.e., porosity and permeability, need to be assigned to generate the synthetic geological computation domain. The porosity range of the geological domain is maintained between 0.2 and 0.4 (Figure 2(e)); the range of porosity considered is with respect to Deccan basalt [6, 60]. The porosity values to each grid cell are assigned randomly by the Gaussian function. The permeability is evaluated for the respective porosity value by utilizing the Carmen–Kozeny relation and assigned to the individual grid cell [34].

$$K = \frac{1}{8\tau A_\vartheta^2}\frac{\varnothing^3}{(1-\varnothing)^2}, \tag{7}$$

where τ represents the tortuosity and A_ϑ is the specific surface area. For basalt formation, the value considered for the tortuosity is 1, and the specific surface area is equal to $2.4 \times 10^5\ \mu\text{m}^{-1}$, which are obtained from A. Navarre-Sitchler et al. [61]. The range of permeability for simulation is evaluated in between 10 and 1500 mD. Figures 2(e) and 2(f) illustrate the porosity and permeability of the geological domain. The hydrostatic boundary conditions are specified for all the outer boundaries except the top surface, which has a no-flow condition. The depth of the synthetic domain starts from 800 m, as illustrated in Figure 2(d). This indicates that the sequestration of CO_2 in the simulation domain is carried out below 800 m from the surface [62, 63]. As the geological domain considered for the simulation is a sloping domain, a uniform initial reservoir pressure cannot be taken for the whole simulation domain. The synthetic domain modeled is the sloping landscape, so the depth value "h" for each grid cell changes. The initial reservoir pressure for each grid cell varies depending on the depth of the grid. The initial reservoir pressure in the reservoir is calculated by $\rho_w gh$. As the density of water considered in the geological domain is constant, the pressure is dependent only on the depth factor, h. The reservoir pressure varies from 0.707 to 22.068 MPa in the geological domain.

3.3. Trapping Capacity Calculation. The flow in the reservoir domain is characterized using conservation of mass, a modified Darcy's law, based on the concept of relative permeability. The entrapment percentage calculations are performed based on the porosity, pore-volume, and CO_2 saturation of the grid cells. Further in the text, the word entrapment percentage means the total trapping percentage (both structural and residual trapping percentages). Structural trapping is calculated using the following formula:

$$\text{Structural trapping} = \sum_{n=1}^{nf}\left(\varnothing V_s \rho_{co_2}\right) \times \min\left(S_{co_2}, S_{rco_2}\right). \tag{8}$$

Residual trapping is calculated using the following formula:

$$\text{Residual trapping} = \sum_{n=1}^{nf}\left(\varnothing V_r \rho_{co_2}\right) \times \min\left(S_{co_2}, S_{rco_2}\right). \tag{9}$$

The movable plume is the remaining quantity of CO_2 after the structural and residual trapping. The term nf is the

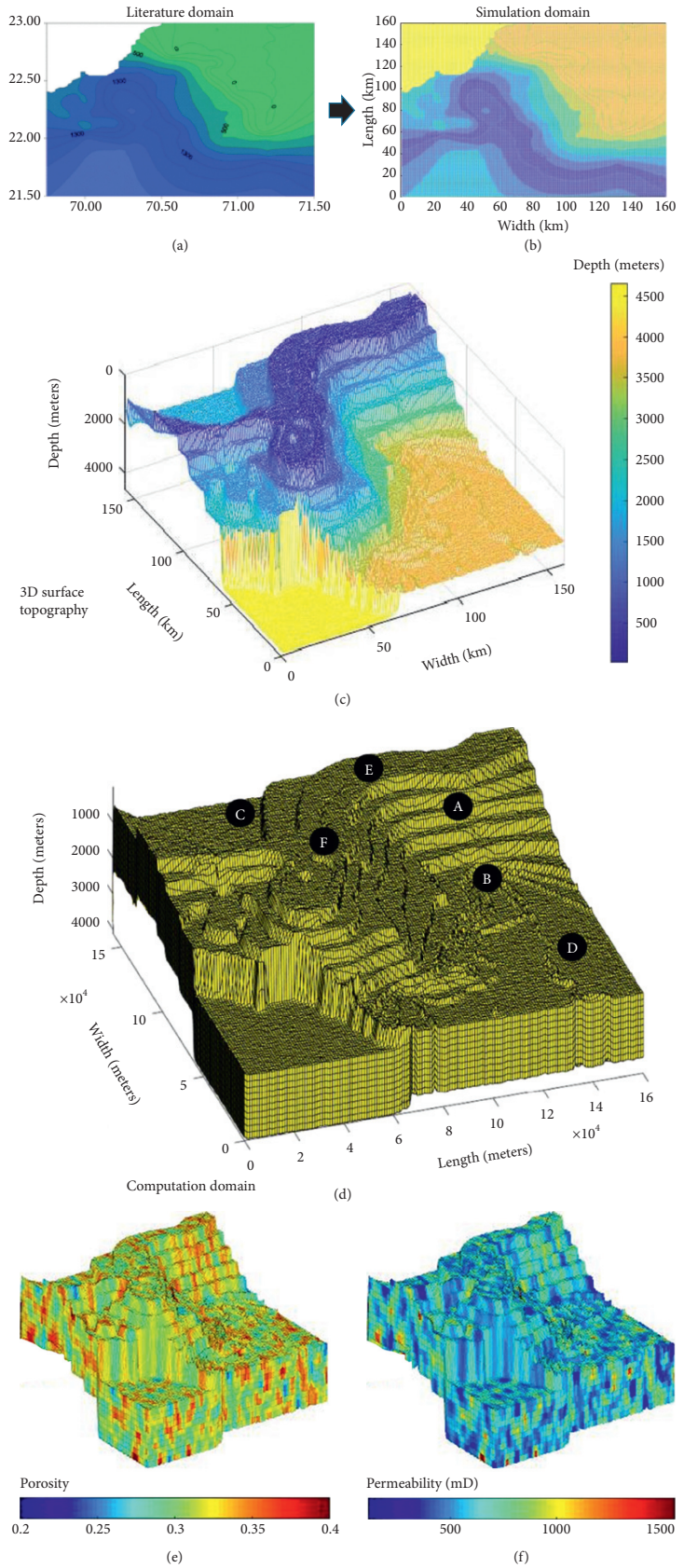

FIGURE 2: The illustration of (a) contour plot, showing the thickness of the Deccan trap in Saurashtra region, Gujarat [19]; (b) numerically modeled synthetic simulation domain; (c) three-dimensional view of simulation domain; (d) 3D discretization after upscaling and discrete points, representing the CO_2 injection points; (e) the porosity; and (f) permeability variation of the synthetic domain considered for CO_2 geologic sequestration simulation.

total number of cells in the grid structure. S_{CO_2} and S_{rCO_2} are the saturation of CO_2 and residual CO_2 saturation. V_s and V_r are the cell volumes of structural traps and residual traps, respectively. The structural traps are identified by analyzing the top surface. The top surface is modeled using the mesh grid. The top surface mesh contains 160×160 grid cells. The MATLAB Gaussian noise function is used to integrate the perturbation into the mesh surface. Now, the numerical differences between each cell of the mesh surface are identified. The structural traps are then identified, and the consecutive cells are saved under structural trapping cells and analyzed during simulations. The remaining cells other than the structural trapping cells of a domain are the active cells for residual trapping calculation. Only the immobile CO_2 saturation cells are considered for the entrapment calculation. The remaining cell saturations are considered for the movable plume calculations.

4. Simulation Results

4.1. Base Case Scenario. In this section, a numerical simulation is presented for the base case scenario of injecting CO_2 at point B (see Figure 2)(a) of the synthetic computation domain. The CO_2 injection is carried out continuously for the first 20 years at the volumetric flow rate of $99 \times 10^5\ m^3$/day and the pressure of 22.068 MPa. The density and viscosity of water are $975.86\ kg/m^3$ and 0.3086×10^{-3} Pa s and those of CO_2 are $686.54\ kg/m^3$ and 0.0566×10^{-3} Pa s, respectively [34]. Simulations were conducted for 3000 years to observe the structural and residual trapping phenomenon. The geological domain consists of a different range of perturbation cognates, with a peak characteristically referred to as an anticline dome in geology. The fate of CO_2 due to structural and residual trapping in the geological domain is thoroughly analyzed and illustrated in Figure 3, which consists of two congener results. The first column represents the CO_2 saturation in the transparent 3D domain, which can analyze the spreading and displacement of CO_2 in the geological domain. The second column illustrates the saturated CO_2 height in the domain. For an economically adhered CO_2 sequestration project, the lateral spreading should be high during the initial period so that it can cover a large volume of the geological domain. This sizeable spreading can influence the economics of CO_2 sequestration in a virtuous way by reducing the number of injection points.

The histogram plot, Figure 4, represents the percentages of structural trapping, residual trapping, and movable plume over a geological time scale. In this particular result, it is observed that the CO_2 plume that is formed after CO_2 injection has moved towards the highest elevation region of an anticline dome. The movement was rapid until the injection period (20 years); this is because the injection force also acts on the CO_2 plume, in addition to the buoyancy forces. The CO_2 plume reaches the highest elevation of the anticline dome within 500 years, but to spread through the anticline top surface, it takes about 2500 years. From this specific observation, it can be suggested that the injection force plays a vital role in the lateral spreading of the CO_2 plume during the preliminary phase of CO_2 injection. During the post-injection period, in the absence of injection pressure, the movement of CO_2 slows down drastically. The movable plume, which is then in the significant portion, transforms into structural trapping and residual trapping (see Figure 4). After a protractive time, there might be a possible transformation of structural trapping into residual trapping. This phenomenon of percentage increase in structural trapping and residual trapping over a geological time scale is observed in Figure 4. The increase in the percentage of residual CO_2 will significantly facilitate the coexistence of CO_2 with water to favor the dissolution of CO_2 to instigate solubility trapping phenomena.

4.2. Influence of Injection Location. The injection location in the geological domain plays a significant role in the CO_2 entrapment in the domain. Figure 5 shows the dynamic evolution of the CO_2 trapping during pre- and postinjection periods at each injection point. From Figure 5, two keen observations are noticed; i.e., movable plume gradually decreases over a geological time scale. Also, structural trapping and residual trapping are increasing over the geological time scale. The order of increment of structural trapping and residual trapping is different for all the injection points. This difference is due to the topographical variation of the Deccan traps.

The modeled domain is categorized into three parts to explain the influences of the Deccan trap topographical variation. The first part of categorization is the flat bottom of the domain, the second categorized part is the sloping stairsteps traps of the domain, and the third part is the highest elevation of the structural domain. When the CO_2 is injected at the highest elevation point at injection points C, E, and F, as illustrated in Figure 6, due to the low availability of migration volume and traps, the trapping percentage recorded is low, as observed in Figure 5.

Two injection points are selected to elucidate the influences of the sloping traps. One injection point is at the lowest point of the sloping traps (B injection point, see Figure 2(d)), and another one is located at the top section of sloping traps (A injection point, see Figure 2(d)). The results show that the entrapment percentage recorded at injection point B is highest compared to all injection points. When the CO_2 is injected at the lowest point, the CO_2 spends more time migrating upwards. During this process, the plume encounters a greater number of traps than the A injection point. Thus, the A injection point has a low total entrapment percentage compared to injection point B despite injecting on the sloping trap region, as illustrated in Figure 5. When the CO_2 is injected at the flat bottom (at injection point D), the CO_2 does not undergo as much migration as the B injection point. The lateral spreading of the CO_2 plume for the D injection point highly depends on the injection force. However, for the B injection point addition to the injection force, the sloping nature of the domain helps achieve greater migration and lateral spreading.

By the end of 3000 years for the cases of A, B, C, and D injection points, the total entrapment percentage is

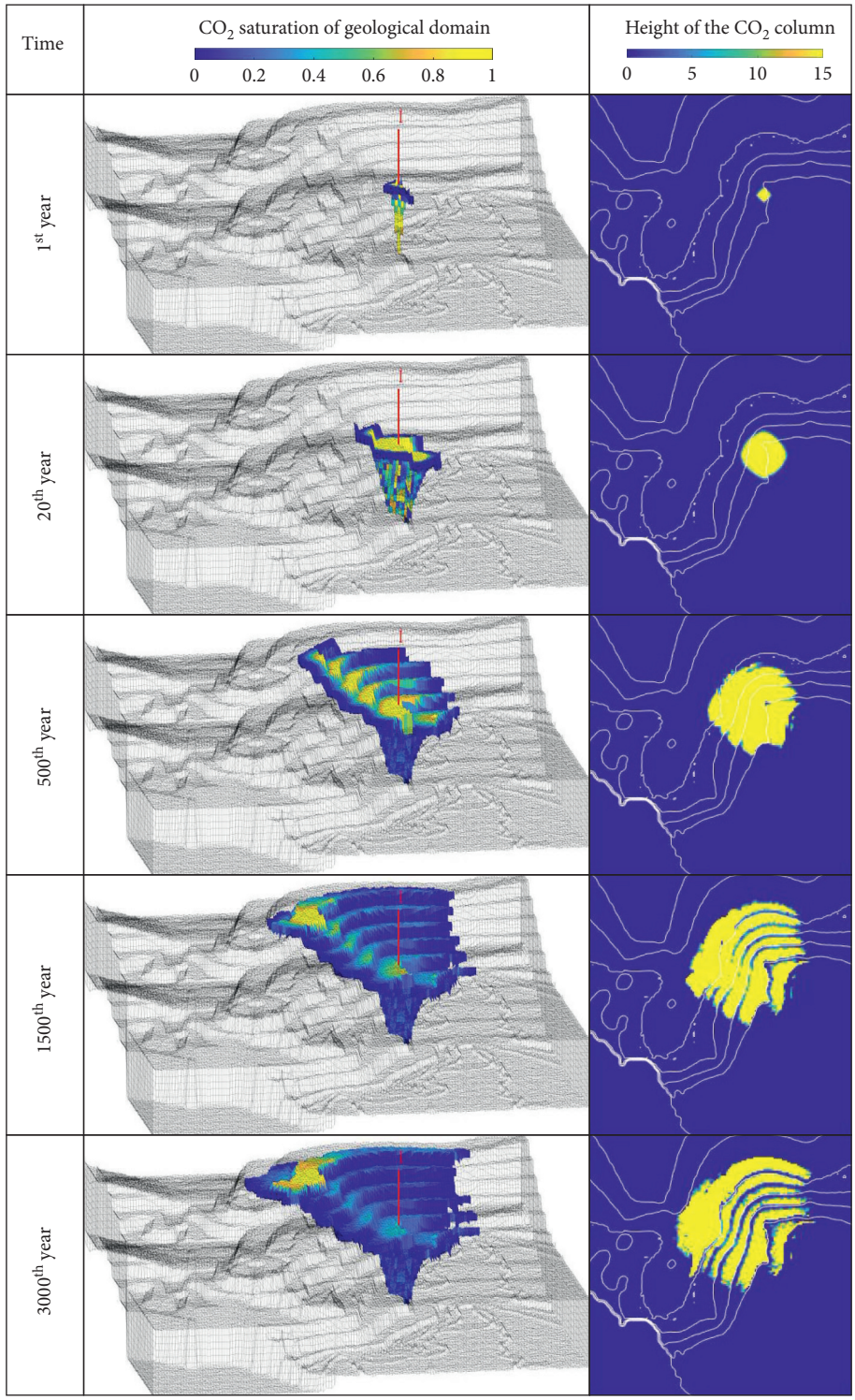

FIGURE 3: The fate of CO_2 during the structural and residual trapping phenomena over geological time represented in the form of (i) height of the saturated CO_2 from the surface; (ii) CO_2 saturation in the 3D domain. Total 7.227×10^{10} m^3 of CO_2 injected for initial 20 years.

dominating compared to the E and F injection points (see Figure 5). This is due to the position of injection points, where more quantity of CO_2 undergoes migration and entrapment. The injection point, which is far away from the anticline dome, takes a lot more time in the migration, and for this reason, the movable plume will reduce over time. From this significant observation, it is understood that positioning the injection points near the sloping traps region yields a higher amount of entrapment (both structural and residual trapping) due to higher CO_2 migration. However, when the CO_2 is injected at the top of the anticline, the decline of lateral movement of CO_2 plume took place, due to

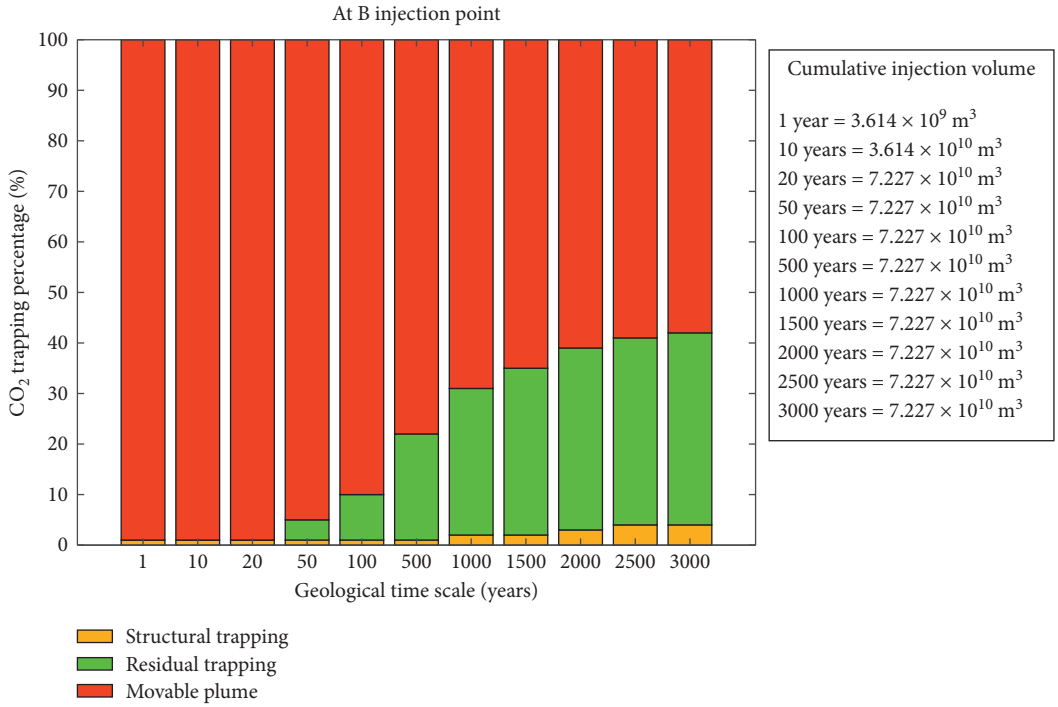

Figure 4: Histogram representing the percentage of CO_2 in the form of structural trapping, residual trapping, and movable plume. It is observed that the structural trapping and residual trapping contributions are increasing during the postinjection period.

which lower percentage entrapment is recorded (see Figure 5). The above explanation shows that the topographical variation and injection point selection are important in implementing CO_2 geological sequestration.

4.3. Influence of Deccan Traps Topography. The naturally available Deccan traps contain geological sloping stairsteps traps, which are integrated and form an anticline structure. In the present synthetic computation domain, these traps are elevated (highlighted in white in all surface plots in Figure 6) into the direction of an enormous anticline dome. From the results of various injection points, as shown in Figure 6, it can be seen that from the injection point (highlighted dark red point), the CO_2 plume is moving towards the highest elevation point. It means that the elevation of the anticline dome dominates the injected CO_2 to move through the sloping traps. When the CO_2 moves through these sloping traps, a higher amount of CO_2 is expected to get trapped in this region. This illustration of trapping on the Deccan traps can be seen in Figure 6 at the B injection point. The higher the amount of CO_2 gets trapped at this structure, the higher the solubility and mineral trapping mechanism entrapment are expected in the long run.

From these observations, it can be concluded that the naturally available topography segments like stairsteps geological traps and perturbation of the geological domain have a significant impact on the structural and residual trapping mechanisms of CO_2 storage in the geological formation. These observations give a glimpse of the importance of selecting the geological site based on geological arrangements and topography.

4.4. Influence of Injection Rates on Structural and Residual Trapping. The influence of injection rates on the trapping mechanisms presented in a histogram plot of the trapping percentage is shown in Figure 7. As the injection rate decreases, the results show that the structural and residual trapping contributions increase, while there is a significant decrease in movable plume contribution. Because the geological domain consists of a finite number of traps, a higher amount of CO_2 is injected into the domain if the injection rate increases. Still, only a finite amount of CO_2 plume can be trapped in the geological domain. The remaining amount of plume will freely move in the domain. For this reason, as the injection rate decreases, the trapping percentage is slightly observed to give an increasing trend and, in contrast, movable plume is decreasing. During the simulations, it was observed that, above 99×10^5 m^3/day injections rate, there is no considerable increase in the structural and residual trapping volume of CO_2. In CO_2 sequestration, the structural and residual trapping mechanisms play a significant role in facilitating the interaction with the aqueous phase for solubility and mineral trapping mechanisms. Therefore, the dominant presence of more structural and residual trapping than movable plume at any time for any point of injection represents the favorable CO_2 sequestration; see also Figure 5 and therein Figure 7 for percentage contributions.

4.5. Effect of Petrophysical Properties on Sweeping Efficiency. A simulation analysis is conducted to study the effects of porosity and permeability on the sweeping efficiency of the geological domain. This study will understand the impact of CO_2 sequestration in the Deccan traps at a low range of

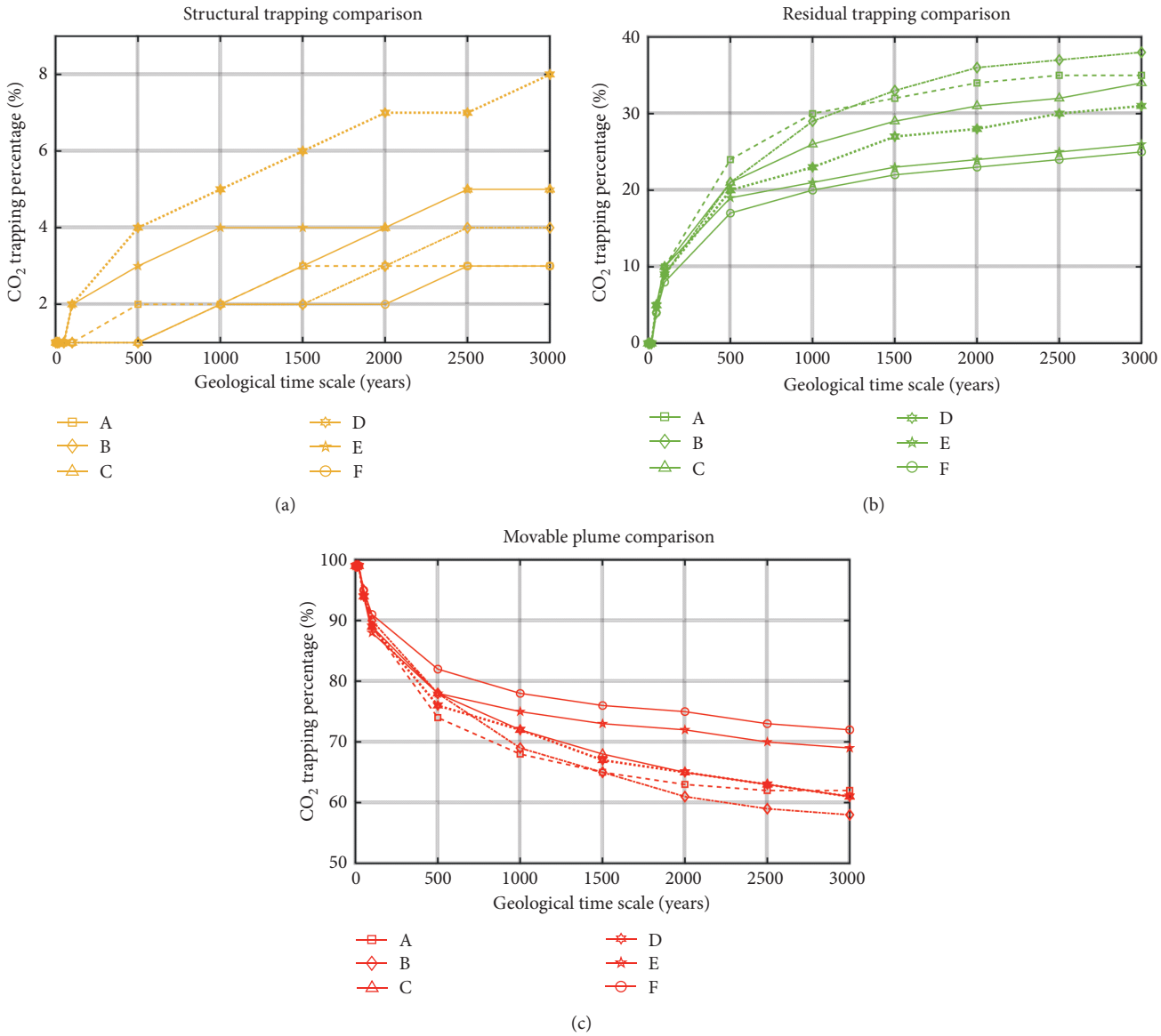

Figure 5: Dynamic evolution of structural trapping and residual trapping when CO_2 is injected at points A, B, C, D, E, and F of the synthetic geological domain.

petrophysical properties. The two sets of porosity and permeability ranges are considered in these simulations. These simulations are carried out at injection point B with the injection rate of 99×10^5 m^3/day, which is continued up to the initial 20 years. The remaining 2980 years are reserved for postinjection analysis. The porosity ranges for simulation set 1 are considered between 0.05 and 0.1, and the permeability range is between 1 and 10 mD. The range of porosity and permeability for simulation set 2 is considered from 0.2 to 0.4 and 10 to 1500 mD, respectively.

The sweeping efficiency deals with the amount of lateral spreading of nonwetting or injected CO_2 into the geological domain. As the lateral spreading increases, the sweeping efficiency of the CO_2 also increases, which will reduce the required number of injection points in the establishment of CCS. Ultimately, this will have a positive impact on the financial aspects of the implementation of CO_2 sequestration projects. From Figure 8(a), it is observed that the simulation set 1 has lower sweeping efficiency than the simulation set 2 for 99×10^5 m^3/day injection rate at injection point B. This variation in the sweeping efficiency is due to the different petrophysical properties used for both simulation sets. Due to the low petrophysical properties range in the simulation set 1, the injected CO_2 will experience high restriction while percolating through the porous domain, and this will reduce the lateral spreading of the CO_2 in the geological domain. As the lateral spreading and plume displacement are low, the percentage of CO_2 entrapment for the structural and residual trapping will be recorded less over geological time. As the CO_2 plume movement is low, it will take time to explore the traps in the geological domain. This phenomenon can be seen in the histogram plots of Figure 8(b), where the

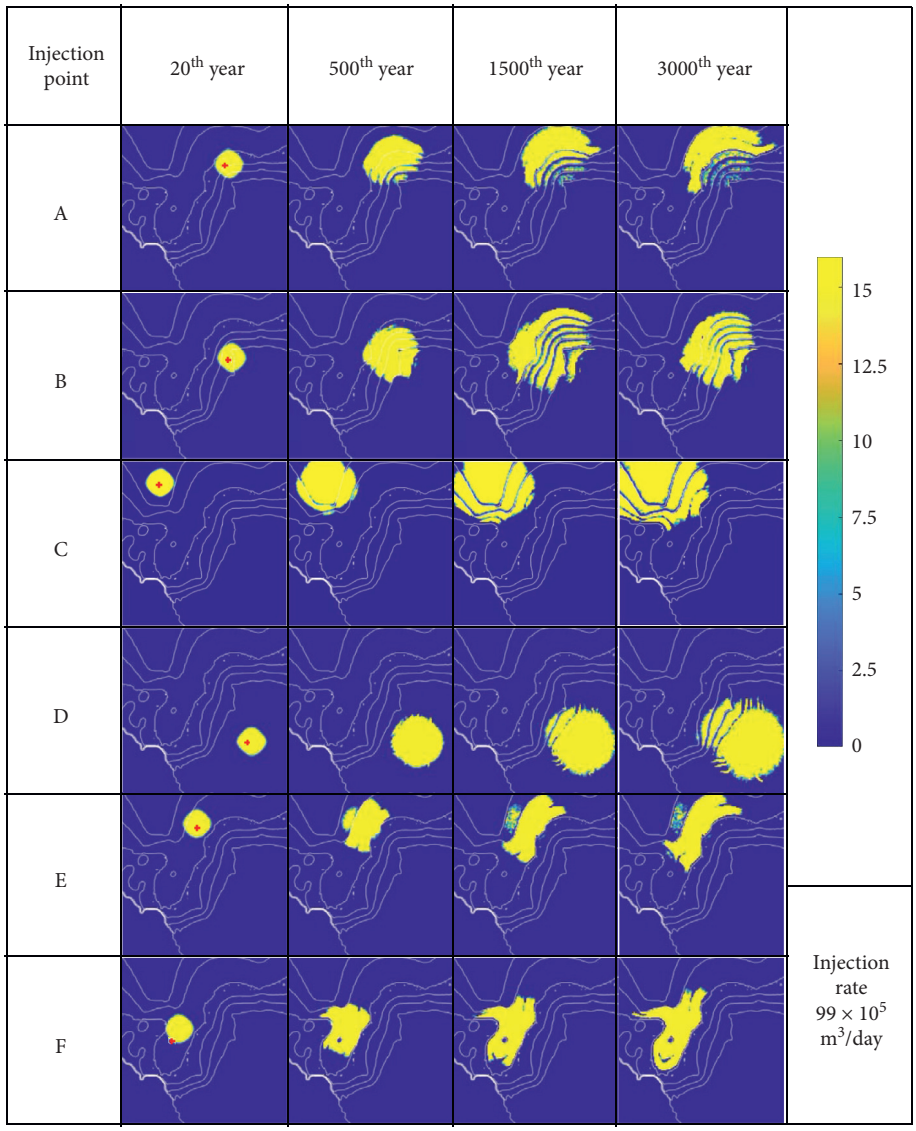

Figure 6: Influence of Deccan traps topography on structural and residual trapping. The illustration represents the movement of CO_2 when injecting at various points in the computation domain.

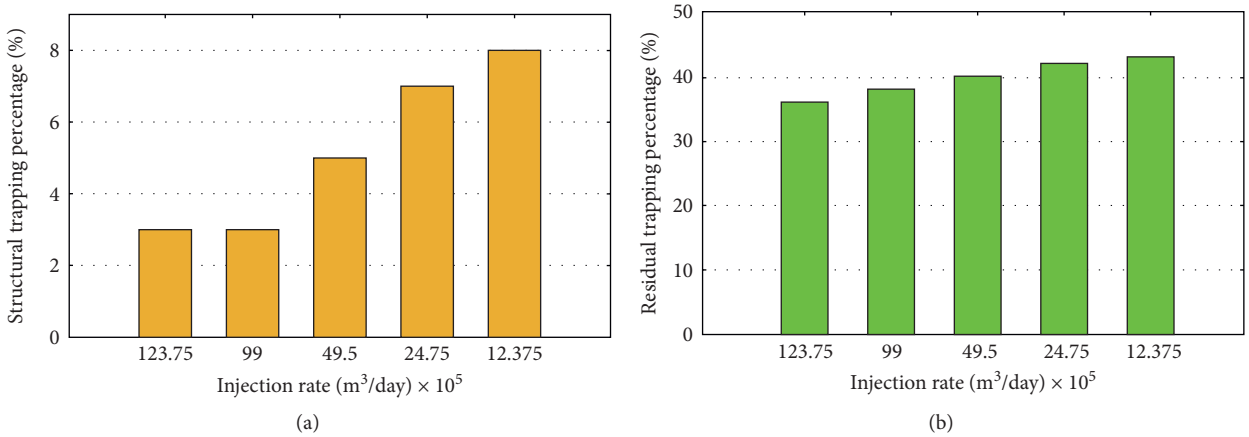

Figure 7: Continued.

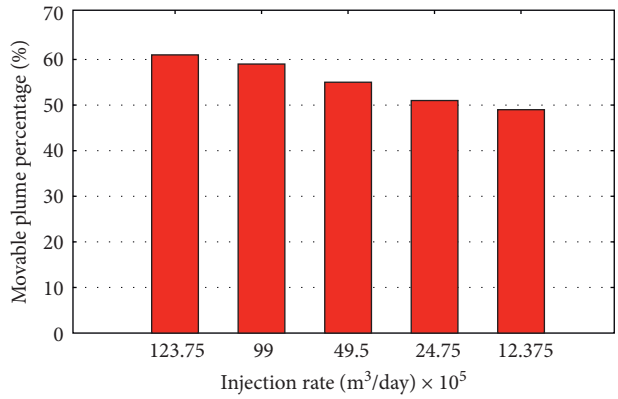

(c)

Figure 7: Illustration of (a) structural trapping, (b) residual trapping, and (c) movable plume at injection point B for varying injection rates 123.75×10^5, 99×10^5, 49.5×10^5, 24.75×10^5, and 12.375×10^5 m^3/day.

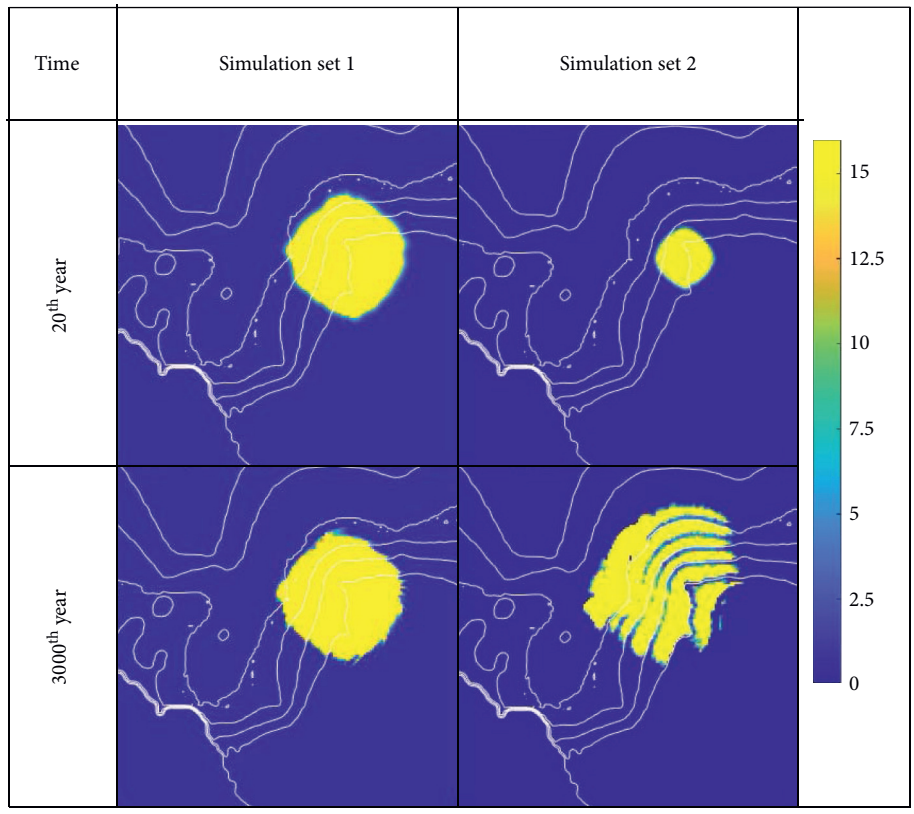

(a)

Figure 8: Continued.

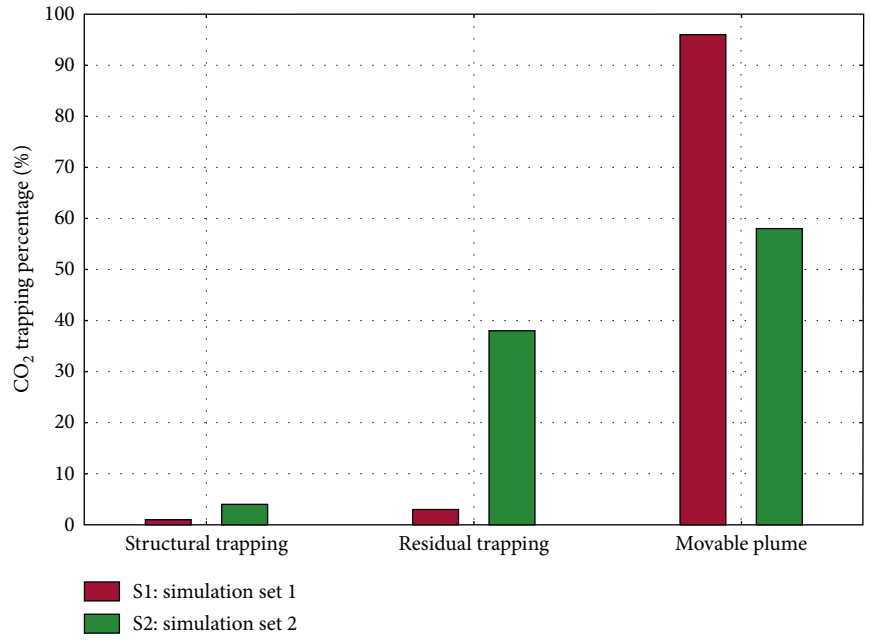

(b)

Figure 8: (a) Sweeping efficiency comparison for different porosity and permeability ranges. (b) Comparison of the percentage of structural trapping, residual trapping, and movable plume between the two petrophysical ranges.

structural and residual trapping percentages for the geological time are illustrated at the end of the 3000^{th} year.

The percentage of entrapment recorded for the structural and residual trapping provides a clear indication of the sweeping efficiency. In simulation set 2, as the CO_2 lateral movement (sweep efficiency) is high compared to that in the simulation set 1, more CO_2 will percolate and explore more traps of a computational domain and get structurally and residually trapped. Due to this, the structural and residual trapping entrapment percentages are recorded high in simulation set 2 when compared to simulation set 1; these results are clearly illustrated in Figure 8(b). In simulation set 1, due to the low range of petrophysical properties, the lateral movement of injected CO_2 is low in the geological domain. The movable plume dominates compared to simulation set 2. The low lateral movement of CO_2 in the geological sequestration process due to the low petrophysical properties range can affect the structural integrity of the geological domain. Even if the structural arrangement of geological storage is not affected, the strangled CO_2 will undergo solubility and mineral reaction in the region. In the mineral reactions, if the dissolution reaction dominates, it may weaken the injection well point and the surrounding region; if the precipitation reactions dominate, it may affect the storage capacity due to decreasing porosity.

5. Conclusions

This study investigates the possible implementation of CO_2 geological sequestration in the Deccan volcanic province of the Saurashtra region, Gujarat. The numerical analysis is carried out to analyze the influences of specific sequestration parameters, such as the petrophysical properties, injection rate, and the injection point. Utilizing the optimal injection rate at an optimal injection point can result in maximum storage for a more extended period without compromising the caprock integrity. Structural and residual trapping mechanisms contribute significantly to store CO_2 for a relatively significant period. In this simulation analysis, it is observed that the percentage of structural trapping and residual trapping is increasing by decreasing the injection rates. This trend was consistent at all the injection points due to the finite amount of trap capacity. The dominance of residual trapping depends on the proximity of the formation traps near the injection points, as formation traps act as minireservoirs and contribute significantly to the entire trapping phenomena. Furthermore, this study has demonstrated the structural and residual trapping dependencies on the petrophysical properties. The lower petrophysical properties range of a geological domain has shown a higher restriction for the CO_2 movement. Our preliminary investigations on structural trapping and residual trapping mechanisms are promising for further studies to implement CO_2 sequestration in the Deccan volcanic province. Future works include the reactive transport modeling of solubility trapping and mineral trapping mechanisms on various geological domains of Deccan volcanic province to comprehend the feasibility of CO_2 sequestration.

Data Availability

The data used to support the findings of this study are included within the article.

Conflicts of Interest

The authors declare that they have no conflicts of interest.

Acknowledgments

The authors would like to acknowledge Science and Engineering Research Board (SERB), India, for providing financial support under the Core Research Grant with file no. EMR/2017/02450. The authors would also like to thank SINTEF for making the MATLAB Reservoir Simulation Toolbox (MRST), an open-source code for simulating the structural and residual trapping phenomena.

References

[1] J. Plenio, *Carbon Dioxide Levels Hit New Record; COVID Impact 'a Tiny Blip', WMO Says*, UN News, New York, NY, USA, 2020, https://news.un.org/en/story/2020/11/1078322.

[2] P. Mathieu, "The IPCC special report on carbon dioxide capture and storage," in *ECOS 2006-Proceedings of the 19th International Conference on Efficiency, Cost, Optimization, Simulation and Environmental Impact of Energy Systems*, pp. 1611–1618, Aghia Pelagia, Greece, July 2006.

[3] D. Y. C. Leung, G. Caramanna, and M. M. Maroto-Valer, "An overview of current status of carbon dioxide capture and storage technologies," *Renewable and Sustainable Energy Reviews*, vol. 39, pp. 426–443, 2014.

[4] R. Shukla, P. Ranjith, A. Haque, and X. Choi, "A review of studies on CO_2 sequestration and caprock integrity," *Fuel*, vol. 89, no. 10, pp. 2651–2664, 2010.

[5] T. L. Otheim, L. Adam, K. Van Wijk, M. L. Batzle, T. McLing, and R. Podgorney, "CO_2 sequestration in basalt: carbonate mineralization and fluid substitution," *The Leading Edge*, vol. 30, no. 12, pp. 1354–1359, 2011.

[6] S. B. Deolankar, "The deccan basalts of Maharashtra, India-their potential as aquifers," *Groundwater*, vol. 18, no. 5, pp. 434–437, 1980.

[7] O. P. Pandey, N. Vedanti, and S. S. Ganguli, "Some insights into possible CO_2 sequestration in subsurface formations beneath deccan volcanic province of India," *Journal of Indian Geophysical Union, Special*, vol. 1, pp. 20–25, 2016.

[8] K. S. Jayaraman, "India's carbon dioxide trap," *Nature*, vol. 445, p. 350, 2007.

[9] P. Viebahn, S. Höller, D. Vallentin, H. Liptow, and A. Villar, "Future CCS implementation in India: a systemic and long-term analysis," *Energy Procedia*, vol. 4, pp. 2708–2715, 2011.

[10] K. N. S. S. S. Srinivas, P. P. Kishore, and D. V. S. Rao, "The geological site characterisation of the Mandla region, Eastern Deccan volcanic province, Central India," *Journal of Earth System Science*, vol. 128, no. 5, pp. 1–16, 2019.

[11] P. Krishnamurthy, "Carbonatites of India," *Journal of the Geological Society of India*, vol. 94, no. 2, pp. 117–138, 2019.

[12] B. P. McGrail, H. T. Schaef, A. M. Ho et al., "Potential for carbon dioxide sequestration in flood basalts," *Journal of Geophysical Research: Solid Earth*, vol. 111, no. 12, pp. 1–13, 2006.

[13] W. Xiong, R. K. Wells, J. A. Horner et al., "CO_2 mineral sequestration in naturally porous basalt," *Environmental Science and Technology Letters*, vol. 5, no. 3, pp. 142–147, 2018.

[14] B. Ottens, J. Götze, R. Schuster et al., "Exceptional multi stage mineralization of secondary minerals in cavities of flood basalts from the Deccan volcanic province, India," *Minerals*, vol. 9, no. 6, pp. 1–41, 2019.

[15] A. Kumar, J. P. Shrivastava, and V. Pathak, "Mineral carbonation reactions under water-saturated, hydrothermal-like conditions and numerical simulations of CO_2 sequestration in tholeiitic basalt of the Eastern Deccan volcanic province, India," *Applied Geochemistry*, vol. 84, pp. 87–104, 2017.

[16] P. S. R. Prasad, D. S. Sarma, and S. N. Charan, "Mineral trapping and sequestration of carbon-dioxide in Deccan basalts: SEM, FTIR and Raman spectroscopic studies on secondary carbonates," *Journal of the Geological Society of India*, vol. 80, no. 4, pp. 546–552, 2012.

[17] A. Kumar and J. P. Shrivastava, "Thermodynamic modelling and experimental validation of CO_2 mineral sequestration in Mandla basalt of the Eastern Deccan volcanic province, India," *Journal of the Geological Society of India*, vol. 93, no. 3, pp. 269–277, 2019.

[18] R. J. Rosenbauer, B. Thomas, J. L. Bischoff, and J. Palandri, "Carbon sequestration via reaction with basaltic rocks: geochemical modeling and experimental results," *Geochimica et Cosmochimica Acta*, vol. 89, pp. 116–133, 2012.

[19] D. N. Murthy, K. Veeraswamy, and T. Harinarayana, "Deep geoelectric structure and its relation to seismotectonics of the Saurashtra region, Western India," *Open Journal of Earthquake Research*, vol. 9, no. 2, pp. 181–200, 2020.

[20] D. Zhang and J. Song, "Mechanisms for geological carbon sequestration," *Procedia IUTAM*, vol. 10, pp. 319–327, 2013.

[21] B. Niu, A. Al-Menhali, and S. C. Krevor, "The impact of reservoir conditions on the residual trapping of carbon dioxide in Berea sandstone," *Water Resources Research*, vol. 51, no. 4, pp. 2009–2029, 2015.

[22] R. Allen, H. M. Nilsen, O. Andersen, and K.-A. Lie, "On obtaining optimal well rates and placement for CO_2 storage," *Computational Geosciences*, vol. 21, no. 5–6, pp. 1403–1422, 2017.

[23] S. Bachu, "CO_2 storage in geological media: role, means, status and barriers to deployment," *Progress in Energy and Combustion Science*, vol. 34, no. 2, pp. 254–273, 2008.

[24] P. N. K. De Silva and P. G. Ranjith, "A study of methodologies for CO_2 storage capacity estimation of saline aquifers," *Fuel*, vol. 93, pp. 13–27, 2012.

[25] S. Bachu, "Sequestration of CO_2 in geological media: criteria and approach for site selection in response to climate change," *Energy Conversion and Management*, vol. 41, no. 9, pp. 953–970, 2000.

[26] S. Bachu and J. J. Adams, "Sequestration of CO_2 in geological media in response to climate change: capacity of deep saline aquifers to sequester CO_2 in solution," *Energy Conversion and Management*, vol. 44, no. 20, pp. 3151–3175, 2003.

[27] S. Krevor, M. J. Blunt, S. M. Benson et al., "Capillary trapping for geologic carbon dioxide storage-from pore scale physics to field scale implications," *International Journal of Greenhouse Gas Control*, vol. 40, pp. 221–237, 2015.

[28] L. K. Abidoye, K. J. Khudaida, and D. B. Das, "Geological carbon sequestration in the context of two-phase flow in porous media: a review," *Critical Reviews in Environmental Science and Technology*, vol. 45, no. 11, pp. 1105–1147, 2015.

[29] D. Alexander and D. Boodlal, "Evaluating the effects of CO_2 injection in faulted saline aquifers," *Energy Procedia*, vol. 63, pp. 3012–3021, 2014.

[30] J. E. Beane, C. A. Turner, P. R. Hooper, K. V. Subbarao, and J. N. Walsh, "Stratigraphy, composition and form of the Deccan Basalts, Western Ghats, India," *Bulletin of Volcanology*, vol. 48, no. 1, pp. 61–83, 1986.

[31] K.-A. Lie, H. M. Nilsen, O. Andersen, and O. Møyner, "A simulation workflow for large-scale CO_2 storage in the Norwegian North Sea," *Computational Geosciences*, vol. 20, no. 3, pp. 607–622, 2016.

[32] O. A. Andersen, H. M. Nilsen, and K. A. Lie, "Reexamining CO_2 storage capacity and utilization of the Utsira formation," in *Proceedings of 14th European Conference on the Mathematics of Oil Recovery 2014, ECMOR 2014*, Catania, Italy, December 2014.

[33] H. Møll Nilsen, K.-A. Lie, and O. Andersen, "Analysis of CO_2 trapping capacities and long-term migration for geological formations in the Norwegian North Sea using MRST-co2lab," *Computers and Geosciences*, vol. 79, pp. 15–26, 2015.

[34] K.-A. Lie, *An Introduction to Reservoir Simulation Using MATLAB/GNU Octave*, Cambridge University Press, Cambridge, UK, 2019.

[35] H. Ahn, S. O. Kim, M. Lee, and S. Wang, "Migration and residual trapping of immiscible fluids during cyclic injection: pore-scale observation and quantitative analysis," *Geofluids*, vol. 2020, Article ID 4569208, 13 pages, 2020.

[36] S. Joodaki, Z. Yang, J. Bensabat, and A. Niemi, "Model analysis of CO_2 residual trapping from single-well push pull test based on hydraulic withdrawal tests–Heletz, residual trapping experiment I," *International Journal of Greenhouse Gas Control*, vol. 97, 2020.

[37] C. H. Pentland, *Measurements of non-wetting phase trapping in porous media*, PhD Thesis, Department of Earth Science and Engineering, Royal School of Mines, London, UK, 2010.

[38] Y. Tanino and M. J. Blunt, "Capillary trapping in sandstones and carbonates: dependence on pore structure," *Water Resources Research*, vol. 48, no. 8, pp. 1–13, 2012.

[39] M. Andrew, B. Bijeljic, and M. J. Blunt, "Pore-scale imaging of trapped supercritical carbon dioxide in sandstones and carbonates," *International Journal of Greenhouse Gas Control*, vol. 22, pp. 1–14, 2014.

[40] S. Wang and T. K. Tokunaga, "Capillary pressure-saturation relations for supercritical CO_2 and brine in limestone/dolomite sands: implications for geologic carbon sequestration in carbonate reservoirs," *Environmental Science & Technology*, vol. 49, no. 12, pp. 7208–7217, 2015.

[41] M. Soroush, D. Wessel-Berg, O. Torsaeter, and J. Kleppe, "Investigating residual trapping in CO_2 storage in saline aquifers-application of a 2D glass model, and image analysis," *Energy Science and Engineering*, vol. 2, no. 3, pp. 149–163, 2014.

[42] R. Juanes, E. J. Spiteri, F. M. Orr, and M. J. Blunt, "Impact of relative permeability hysteresis on geological CO_2 storage," *Water Resources Research*, vol. 42, no. 12, pp. 1–13, 2006.

[43] C. Lamy, S. Iglauer, C. H. Pentland, M. J. Blunt, and G. Maitland, "Capillary trapping in carbonate rocks," in *Proceedings of 72nd European Association of Geoscientists and Engineers Conference and Exhibition 2010*, pp. 815–823, Barcelona, Spain, June 2010.

[44] A. Raza, R. Gholami, R. Rezaee et al., "Assessment of CO_2 residual trapping in depleted reservoirs used for geo-sequestration," *Journal of Natural Gas Science and Engineering*, vol. 43, pp. 137–155, 2017.

[45] Y. Pamukcu, S. Hurter, L. Jammes, D. Vu-Hoang, and L. Pekot, "Characterizing and predicting short term performance for the in Salah Krechba field CCS joint industry project," *Energy Procedia*, vol. 4, pp. 3371–3378, 2011.

[46] A. Saeedi, R. Rezaee, and B. Evans, "Experimental study of the effect of variation in in-situ stress on capillary residual trapping during CO_2 geo-sequestration in sandstone reservoirs," *Geofluids*, vol. 12, no. 3, pp. 228–235, 2012.

[47] R. S. Jayne, H. Wu, and R. M. Pollyea, "A probabilistic assessment of geomechanical reservoir integrity during CO_2 sequestration in flood basalt formations," *Greenhouse Gases: Science and Technology*, vol. 9, no. 5, pp. 979–998, 2019.

[48] Z. Yang, Y. F. Chen, and A. Niemi, "Gas migration and residual trapping in bimodal heterogeneous media during geological storage of CO_2," *Advances in Water Resources*, vol. 142, Article ID 103608, 2020.

[49] B. Niu, A. Al-Menhali, and S. Krevor, "A study of residual carbon dioxide trapping in sandstone," *Energy Procedia*, vol. 63, pp. 5522–5529, 2014.

[50] H. Møll Nilsen, K.-A. Lie, O. Møyner, and O. Andersen, "Spill-point analysis and structural trapping capacity in saline aquifers using MRST-co2lab," *Computers and Geosciences*, vol. 75, pp. 33–43, 2015.

[51] M. Angeli, J. I. Faleide, and R. H. Gabrielsen, "Evaluating seal quality for potential storage sites in the Norwegian North Sea," *Energy Procedia*, vol. 37, pp. 4853–4862, 2013.

[52] R. Allen, H. M. Nilsen, K.-A. Lie, O. Møyner, and O. Andersen, "Using simplified methods to explore the impact of parameter uncertainty on CO_2 storage estimates with application to the Norwegian Continental Shelf," *International Journal of Greenhouse Gas Control*, vol. 75, pp. 198–213, 2018.

[53] H. M. Nilsen, A. R. Syversveen, K. A. Lie, J. Tveranger, and J. M. Nordbotten, "Impact of top-surface morphology on CO_2 storage capacity," *International Journal of Greenhouse Gas Control*, vol. 11, pp. 221–235, 2012.

[54] M. Ahmadinia, S. M. Shariatipour, O. Andersen, and M. Sadri, "Benchmarking of vertically integrated models for the study of the impact of caprock morphology on CO_2 migration," *International Journal of Greenhouse Gas Control*, vol. 90, Article ID 102802, 2019.

[55] S. K. Biswas, "Rift basins in western margin of India and their hydrocarbon prospects with special reference to Kutch Basin," *American Association of Petroleum Geologists, Bulletin*, vol. 66, no. 10, pp. 1497–1513, 1982.

[56] H. Gupta, N. Purnachandra Rao, S. Roy et al., "Investigations related to scientific deep drilling to study reservoir-triggered earthquakes at Koyna, India," *International Journal of Earth Sciences*, vol. 104, no. 6, pp. 1511–1522, 2015.

[57] P. S. R. Prasad, D. Srinivasa Sarma, L. Sudhakar et al., "Geological sequestration of carbon dioxide in Deccan basalts: preliminary laboratory study," *Current Science*, vol. 96, no. 2, pp. 288–291, 2009.

[58] J. J. Mahoney, H. C. Sheth, D. Chandrasekharam, and Z. X. Peng, "Geochemistry of flood basalts of the Toranmal section, Northern Deccan Traps, India: implications for regional Deccan stratigraphy," *Journal of Petrology*, vol. 41, no. 7, pp. 1099–1120, 2000.

[59] P. O. Alexander and M. K. Purohit, "Giant Plagioclase basalt from the Deccan Volcanic Province (DVP), Sagar district, Madhya Pradesh, India: first report and implications," *Journal of the Geological Society of India*, vol. 94, no. 2, pp. 139–141, 2019.

[60] K. J. Prasanna Lakshmi, P. Senthil Kumar, K. Vijayakumar et al., "Petrophysical properties of the Deccan basalts exposed in the Western Ghats escarpment around Mahabaleshwar and Koyna, India," *Journal of Asian Earth Sciences*, vol. 84, pp. 176–187, 2014.

[61] A. Navarre-Sitchler, C. I. Steefel, L. Yang et al., "Evolution of porosity and diffusivity associated with chemical weathering

of a Basalt clast," *Journal of Geophysical Research: Earth Surface*, Blackwell Publishing Ltd, vol. 114, no. 2, 2009.

[62] H. Herzog and D. Golomb, *Carbon Capture and Storage from Fossil Fuel Use*, Massachusetts Institute of Technology, Cambridge, MA, USA, 2004, https://sequestration.mit.edu/pdf/enclyclopedia_of_energy_article.pdf.

[63] J. J. Dooley, R. T. Dahowski, C. L. Davidson et al., *Carbon Dioxide Capture and Geologic Storage-A Core Element of a Global Energy Technology Strategy to Address Climate Change*, Battelle, Joint Global Change Research Institute (JGCRI), Columbus, OH, USA, 2006, https://www.epa.gov/sites/production/files/2015-05/documents/act_2007_02_battelle.pdf.